Redox Biology 43 (2021) 101989

Contents lists available at ScienceDirect

Redox Biology

journal homepage: www.elsevier.com/locate/redox

Research Paper

Lysosomal nitric oxide determines transition from autophagy to ferroptosis after exposure to plasma-activated Ringer's lactate

Li Jiang [a,1], Hao Zheng [a,1], Qinying Lyu [a], Shotaro Hayashi [a,b], Kotaro Sato [a], Yoshitaka Sekido [c], Kae Nakamura [b,d], Hiromasa Tanaka [d,e], Kenji Ishikawa [d], Hiroaki Kajiyama [b,d], Masaaki Mizuno [e], Masaru Hori [d], Shinya Toyokuni [a,d,f,*]

[a] Department of Pathology and Biological Responses, Nagoya University Graduate School of Medicine, 65 Tsurumai-cho, Showa-ku, Nagoya, 466-8550, Japan
[b] Department of Obstetrics and Gynecology, Nagoya University Graduate School of Medicine, 65 Tsurumai-cho, Showa-ku, Nagoya, 466-8550, Japan
[c] Division of Cancer Biology, Aichi Cancer Center Research Institute, 1-1 Kanokoden, Chikusa-ku, Nagoya, 464-8681, Japan
[d] Center for Low Temperature Plasma Sciences, Nagoya University, Furo-cho, Chikusa-ku, Nagoya, 464-8603, Japan
[e] Center for Advanced Medicine and Clinical Research, Nagoya University Hospital, 65 Tsurumai-cho, Showa-ku, Nagoya, 466-8550, Japan
[f] Sydney Medical School, The University of Sydney, Sydney, NSW, 2006, Australia

ARTICLE INFO

Keywords:
Ferroptosis
Non-thermal plasma-activated Ringer's lactate
Malignant mesothelioma
Nitric oxide
Autophagy

ABSTRACT

Non-thermal plasma (NTP), an engineered technology to generate reactive species, induces ferroptosis and/or apoptosis specifically in various-type cancer cells. NTP-activated Ringer's lactate (PAL) is another modality for cancer therapy at preclinical stage. Here we found that PAL induces selective ferroptosis of malignant mesothelioma (MM) cells, where non-targeted metabolome screening identified upregulated citrulline-nitric oxide (·NO) cycle as a PAL target. ·NO probe detected biphasic peaks transiently at PAL exposure with time-dependent increase, which was responsible for inducible · NO synthase (iNOS) overexpression through NF-κB activation. ·NO and lipid peroxidation occupied lysosomes as a major compartment with increased TFEB expression. Not only ferrostatin-1 but inhibitors for · NO and/or iNOS could suppress this ferroptosis. PAL-induced ferroptosis accompanied autophagic process in the early phase, as demonstrated by an increase in essential amino acids, LC3B-II, p62 and LAMP1, transforming into the later phase with boosted lipid peroxidation. Therefore, ·NO-mediated lysosomal impairment is central in PAL-induced ferroptosis.

1. Introduction

Cancer is a leading and increasing cause of human mortality worldwide (https://www.who.int/news-room/fact-sheets/detail/cancer). Despite recent progress in understanding carcinogenic mechanisms and tumor biology, permanent cure is difficult in advanced cancers of various origins due to the deficiency in available targetable drugs as well as therapy-resistance [1]. Thus, societies persistently require novel modalities for better prognosis of cancer.

Recently, ferroptosis is considered as a biomarker of effectiveness in cancer therapy [2,3]. Cancer cells are intrinsically rich in catalytic Fe(II) for proliferation [4,5], which is now targeted to specifically kill them. Ferroptosis is catalytic Fe(II)-dependent regulated necrosis [6] and immunogenic in comparison to apoptosis [7]. Situations with increased intracellular ratio of iron to sulfur (in association with antioxidants, including glutathione), such as in excess iron or cysteine deprivation, determines the cell fate toward ferroptosis, where lipid peroxidation, especially derived from polyunsaturated phospholipids, finally executes this form of cell death [3,6,8]. Of note, ferroptosis-inducible reagents are demonstrated to strongly correlate with the selective cell death of epithelial-derived cancer cells with highly mesenchymal state [9,10]. Recent studies suggest that dysfunction of intracellular organelles, such as lysosome and mitochondria, under stress conditions contributes to ferroptosis regulation [11].

Malignant mesothelioma (MM) is an aggressive cancer of somatic cavities in association with asbestos exposure [12–14]. Current standard therapeutic regimens for MM have been dismal due to the difficulty in early diagnosis and operational access [15,16]. Non-thermal plasma (NTP) is an engineered technology to generate various reactive species

* Corresponding author. Department of Pathology and Biological Responses, Nagoya University Graduate School of Medicine, 65 Tsurumai-cho, Showa-ku, Nagoya, Japan.
E-mail address: toyokuni@med.nagoya-u.ac.jp (S. Toyokuni).
[1] First co-authors with equal contribution.

https://doi.org/10.1016/j.redox.2021.101989
Received 16 March 2021; Received in revised form 17 April 2021; Accepted 20 April 2021
Available online 23 April 2021

Abbreviations

AAs	amino acids
CE-MS	capillary electrophoresis and mass spectrometry
FACS	fluorescence-activated cell sorter
FBS	fetal bovine serum
Fer-1	Ferrostatin-1
iNOS	inducible nitric oxide synthase (NOS2)
NF-κB	nuclear factor-κB
·NO	nitric oxide
NOS	nitric oxide synthase
NTP	non-thermal plasma
PAL	non-thermal plasma-activated Ringer's lactate
PCA	principal component analysis
pmTOR	phosphorylated mechanistic target of rapamycin (mTOR)
PPP	pentose phosphate pathway
RL	Ringer's lactate
ROS	reactive oxygens species
RT	room temperature
TCA	tricarboxylic acid
TFEB	transcription factor EB

at near body temperature [17–21]. Previously, we showed that direct exposure of NTP specifically kills MM cells in comparison to non-tumorous cells, causing ferroptosis [22,23]. Ferroptosis may be preferred in cancer chemotherapy to apoptosis due to immunogenicity [7] to merit the current availability of immune checkpoint inhibitors [24]. Here we used NTP-activated Ringer's lactate (PAL) to MM cells, considering flexible clinical applications in somatic cavities, and performed comprehensive metabolomic screening in search of the responsible chemical reactions. We report that PAL induces ferroptosis specifically in MM cells, where lysosomal nitric oxide (·NO) plays a critical role in transforming autophagic process into ferroptosis.

2. Materials and methods

2.1. Cell lines and media

Human MM cells, Y-Meso-8A (8A) [25], NCI–H290 as a gift from Dr. Adi F. Gazdar (University of Texas, Southwestern Medical Center) and a human normal mesothelial cell line (LP9) purchased from ATCC (Manassas, VA) were used. Human fibrosarcoma cell line HT1080 was purchased from JCRB (Ibaraki, Osaka, Japan). 8A, H290 and LP9 cells were cultured in RPMI-1640 (189–02025, Wako, Osaka, Japan), containing 10% fetal bovine serum (Biowest; Nuaillé, France) under 5% CO_2 atmosphere. HT1080 cells was cultured in EMEM (051–07615, Wako, Osaka, Japan), containing 10% fetal bovine serum (Biowest; Nuaillé, France) under 5% CO_2 atmosphere.

2.2. Materials

Ringer's lactate solution (Cat. #14500AMZ02080) and Ringer's solution (Cat. #16000AMZ00565) were from Otsuka Pharmaceutical Co., Ltd (Tokyo, Japan). Erastin (Cat. #571203-78-6) [26] was purchased from Cayman Chemical (Ann Arbor, MI). Ferrostatin-1 (Cat. #SML0583) was from Sigma-Aldrich (St. Louis, MO). Carboxy-PTIO (Cat. #C348) [27] was from Dojindo (Kumamoto, Japan). Cisplatin (Cat. #BP809) was from Sigma-Aldrich. 1400 W (Cat. #ab120165) [28] was from Abcam (Cambridge, UK). Balflomycin A1 (Cat. #54645) [29] was purchased from Cell Signaling Technology (Danvers, MA).

2.3. Preparation of PAL

Four distinct PAL solutions were prepared to determine the optimal experimental condition. Briefly, a total of 10 mL of Ringer's lactate solution was placed in 60 mm-diameter culture dishes (Cat. # 430166; Corning). The plasma exposure conditions were identical to those of previously reported experiments [30–33]. Four different compositions of atmospheric gas were applied as 80% Ar either with 20% N_2, 15% N_2+5% O_2, 10% N_2+10% O_2 or 5% N_2+15% O_2 with a closed system (Fuji Corporation, Chiryu, Aichi, Japan). Other conditions were as follows: 10 kV of 60 Hz AC power and gas at a flow rate of 2 standard liters per min. Final PAL was prepared by diluting the original plasma-irradiated lactate solution 14-fold with untreated Ringer's solution.

2.4. Cell viability

In these studies, 5000 cells/well were seeded in 96-well plates (Cat. #167008, Thermo Fisher Scientific) and incubated for 24 h/37 °C. The cells were then treated with PAL for 15 min/37 °C. After incubation in RPMI (5% FBS), the cell count reagent SF (Cat. #07553, Nacalai Tesque, Kyoto, Japan) was used to determine the viability of the cells.

2.5. Calculation of cytotoxicity

Cytotoxicity was assayed by SYTOX™ Green Nucleic Acid Stain (S7020, Thermo Scientific) or LDH assay. In Sytox Green nucleic acid stain assay, 10^5 cells/well were seeded in 12-well plates (Cat. #167008, Thermo Fisher Scientific) and incubated for 24 h/37 °C. The cells were then treated with PAL for 15 min/37 °C. After a 6 h/37 °C incubation in RPMI (5% FBS), the cells were stained with 2.5 μM SYTOX Green and the number of positive cells were observed by a BZ9000 immunofluorescent microscopy, and measured by a Gallios Flow Cytometer (Beckman Coulter) using three technical replicates per sample. In LDH Assay, 5000 cells/well were seeded in 96-well plates (Cat. #167008, Thermo Fisher Scientific) and incubated for 24 h/37 °C. The cells were then treated with PAL for 15 min/37 °C. After incubation in RPMI (5% FBS), the Cytotoxicity LDH Assay Kit-WST (Cat. # CK12, Dojindo, Japan) was used to determine the viability of the cells.

2.6. Metabolomic profiling

Five groups were designed (N = 3) both for Y-Meso-8A (8A) and H290 MM cells: RPMI with 10% FBS (as initial), PAL-untreated Ringer's lactate (RL) solution (as control), PAL, PAL + Fer-1 or erastin. After 5 min's incubation with PAL, cells were treated with or without Fer-1 in RL for 4 h. Cells in the erastin-group were incubated in RL. After 4 h-incubation, extracellular proteins were removed by washing with 10 mL of 5% (w/v) D-mannitol solution while retaining intracellular metabolites. Methanol metabolite extraction was performed according to the human metabolome technologies (HMT, Tsuruoka, Japan) metabolite extraction method for adherent cells. Metabolite concentrations were normalized to viable cell counts. Triplicate supernatants of each sample were analyzed using capillary electrophoresis and mass spectrometry (CE-MS) with a fused silica capillary (50 μm × 80 cm) column. Cations were detected using a CE-time-of-flight MS system (Agilent Technologies) at a positive voltage of 27 kV. Anions were detected using an Agilent 6460 TripleQuad LC/MS QqQ1 CE-MS system at a positive voltage of 30 kV. Data processing and analysis of metabolite levels were performed as follows. Principal component analysis (PCA) was performed to identify global trends among the variables while ignoring outliers. A heatmap was generated by normalization using the mean and standard deviation of individual metabolite measurements across samples. Missing data were imputed as zero. Hierarchical clustering based on Pearson's correlation was performed on the log-transformed normalized data after median centering per metabolite. Statistical

analyses were carried out using Welch's *t*-test, with P values < 0.05 considered significant.

2.7. Transmission electron microscopy

H290 MM cells pre-treated with PAL for 15 min/37 °C. After 4 or 24 h/37 °C incubation with or without Fer-1 in RPMI (5% FBS), cells were harvested and fixed with 2 mM glutaraldehyde in 1 mM PBS as previously described [34]. Transmission electron microscopy was performed with a JEM-1400PLUS (JEOL, Tokyo, Japan).

2.8. Intracellular.NO measurements

The concentration of · NO was measured using diaminofluorescein-FM diacetate (DAF-FM DA, Cat. #SK1004-01; Goryo Chemical Inc., Sapporo, Japan) probe [35] by Gallios Flow Cytometer (Beckman Coulter), using three technical replicates per sample. The fluorescent images were taken with a Zeiss confocal microscope (LSM880; Carl Zeiss, Oberkochen, Germany).

2.9. Intracellular peroxynitrite measurements

The concentration of peroxynitrite was measured using peroxynitrite assay kit (Cat. #ab233468, Abcam). The fluorescent signal was monitored at Ex/Em = 490/530 nm by a Cytation microplate reader using three technical replicates per sample.

2.10. Intracellular ROS measurements

The concentration of peroxides and lipid peroxidation was measured, respectively, using CM-H2DCFDA (Cat. #D399, Thermo Fisher Scientific) [36] and BODIPY™ 581/591 C11 (Cat. #D3861, Thermo Fisher Scientific) [37] by FACS analysis. Fluorescent images were taken with a LSM8800 confocal microscope.

2.11. Protein extraction and immunoblotting

Prior to PAL treatment, MM cells (2.5×10^5) or non-tumorous mesothelial cell LP9 (1×10^6) were plated onto 60-mm dishes and incubated for 48 h/37 °C. After treatment with PAL, cells were then incubated for 24 h/37 °C in complete medium, subsequently collected and lysed to extract proteins. The primary antibodies used for immunoblotting were against iNOS (Cat. #CXNFT; 1/200 dilution; Invitrogen), eNOS (Cat. #9572; 1/500 dilution; Cell Signaling Technology, Danvers, MA), nNOS (Cat. #4234; 1/800 dilution; Cell Signaling Technology), LAMP1 (Cat. #D2DD11; 1/500 dilution, Cell Signaling Technology), and LC3B (Cat. #D11, 1/1000 dilution; Cell Signaling Technology), SQSTM1/p62 (Cat. #D5L7G, 1/1000 dilution; Cell Signaling Technology), mTOR (Cat. #7C10, 1/1000 dilution; Cell Signaling Technology), Phospho-mTOR (Ser2448) (Cat. #D9C2, 1/300 dilution; Cell Signaling Technology) and Keap1 (Cat. #ab139729, 1/1000 dilution; Abcam). Antibodies against β-actin (Cat. #clone AC-15; 1/5000 dilution; Sigma) was used as protein-loading controls. Quantification of the bands was performed with ImageJ 4.7v software (NIH, Bethesda, MD).

2.12. Immunofluorescence using confocal microscopy

After H290 and 8A cells were treated with PAL, they were then incubated for 8 h/37 °C. The cells were then fixed with 4% (w/v) paraformaldehyde for 10 min/RT, washed 3 times using PBS, incubated with 0.1% (v/v) Triton X100 and blocked for 1 h at RT with 3% (w/v) bovine serum albumin. The cells were then incubated overnight at 4 °C with primary antibodies against iNOS (Cat. #CXNFT; 1/200 dilution; Invitrogen), p65 (Cat. #D14E12; 1/400 dilution; Cell Signaling Technology), LAMP1 (Cat. #ab25630; 1/500 dilution; Abcam), LC3B (Cat. #D11; 1/1000 dilution; Cell Signaling Technology), SQSTM1/p62 (Cat. #D5L7G, 1/1000 dilution; Cell Signaling Technology), TFEB (Cat. #1337-I-AP, 1/100 dilution; Proteintech) and NF-κB (Cat. #PA5-88084, 1/500 dilution; Thermofisher), washed 3 times with PBS and incubated with the secondary antibodies, Alexa Fluor® Plus 488 or Alexa Fluor® Plus 568 (Invitrogen). A Zeiss confocal microscope (LSM880, Carl Zeiss) was used to observe cellular morphology. The fluorescence intensity and Mander's overlap for image co-localization were measured using ImageJ 4.7v software. Fifty cells were quantified with ImageJ software for integration of each fluorescence (wavelength) area via excluding the cellular background. Relative intensities per cell in arbitrary units are shown.

2.13. Statistics

All statistical analyses were performed with GraphPad Prism 5 software (GraphPad Software, La Jolla, CA). Significance of difference was determined by unpaired *t*-test, one-way ANOVA or two-way ANOVA, followed by Tukey's multiple comparison test. Significance was defined as $P < 0.05$.

3. Results

3.1. NTP-activated Ringer's lactate (PAL) induces ferroptosis selectively in MM cells

To assess the efficacy and selectivity with different preparations of PAL, LP9 human mesothelial cells and NCI–H290 (H290; derived from sarcomatoid subtype)/Y-MESO-8A (8A; derived from epithelioid subtype) human MM cells were treated with PAL, prepared with different N_2/O_2 ratio as the atmosphere of plasma source. PAL prepared with 10% N_2/10% O_2/80% Ar atmosphere exhibited significant anti-proliferative effects on MM cells without disturbing the proliferation of LP9 normal mesothelial cells (Fig. 1A and B). Of note, whereas sarcomatoid subtype (H290) MM cells exhibited more aggressive behavior in comparison to epithelioid subtype (8A) MM cells (Supplementary Fig. 1A), H290 cells were more sensitive to PAL-induced mortality than 8A cells (Fig. 1B, C, D; Supplementary Fig. 1B, C, D). To determine whether ferroptosis is involved in PAL-induced mortality, cells were treated with PAL for 15 min and the cell viability was examined after an incubation up to 24 h/37 °C in RPMI1640 (5% FBS) with a ferroptosis inhibitor, ferrostatin-1 (Fer-1; 5 μM). PAL induced significant cell death selectively in H290 and 8A cells, which Fer-1 prevented (Fig. 1C). In contrast, Fer-1 failed to reverse cell death induced by cisplatin (20 μM), a chemotherapeutic widely used for the treatment of MM via apoptosis induction (Fig. 1D and E and Supplementary Fig. 1E). Finally, transmission electron microscopy revealed that H290 cells after PAL treatment exhibited deformed mitochondria with vacuoles and dense deposits while nuclear membrane was intact with no nuclear fragmentation (Fig. 1F). These results indicated significant and selective cytotoxicity of PAL to MM cells with the involvement of ferroptosis.

3.2. Metabolome analysis identified both similarities to and differences from erastin-induced ferroptosis

Considering the selective ferroptosis-inducing ability of PAL in MM cells, we performed metabolome analysis to understand the molecular mechanisms involved. Supplementary Fig. 2A shows a schematic illustration of the experimental protocol. Metabolomic profiling using 8A and H290 cells revealed characteristic differences in 116 metabolites among the samples (N = 3) in complete RPMI1640 medium (as initial), Ringer's lactate solution only (RL; as control), PAL, PAL with 5 μM Fer-1 or RL with 5 μM erastin, a cysteine deprivation-type ferroptosis inducer [26] (Supplementary Figs. 2B and 3). Score plots of the principal component analysis (PCA) revealed that PC1 and PC2 can explain 41.7% and 14.4% of the variation, respectively (Fig. 2A). Top-40 metabolites

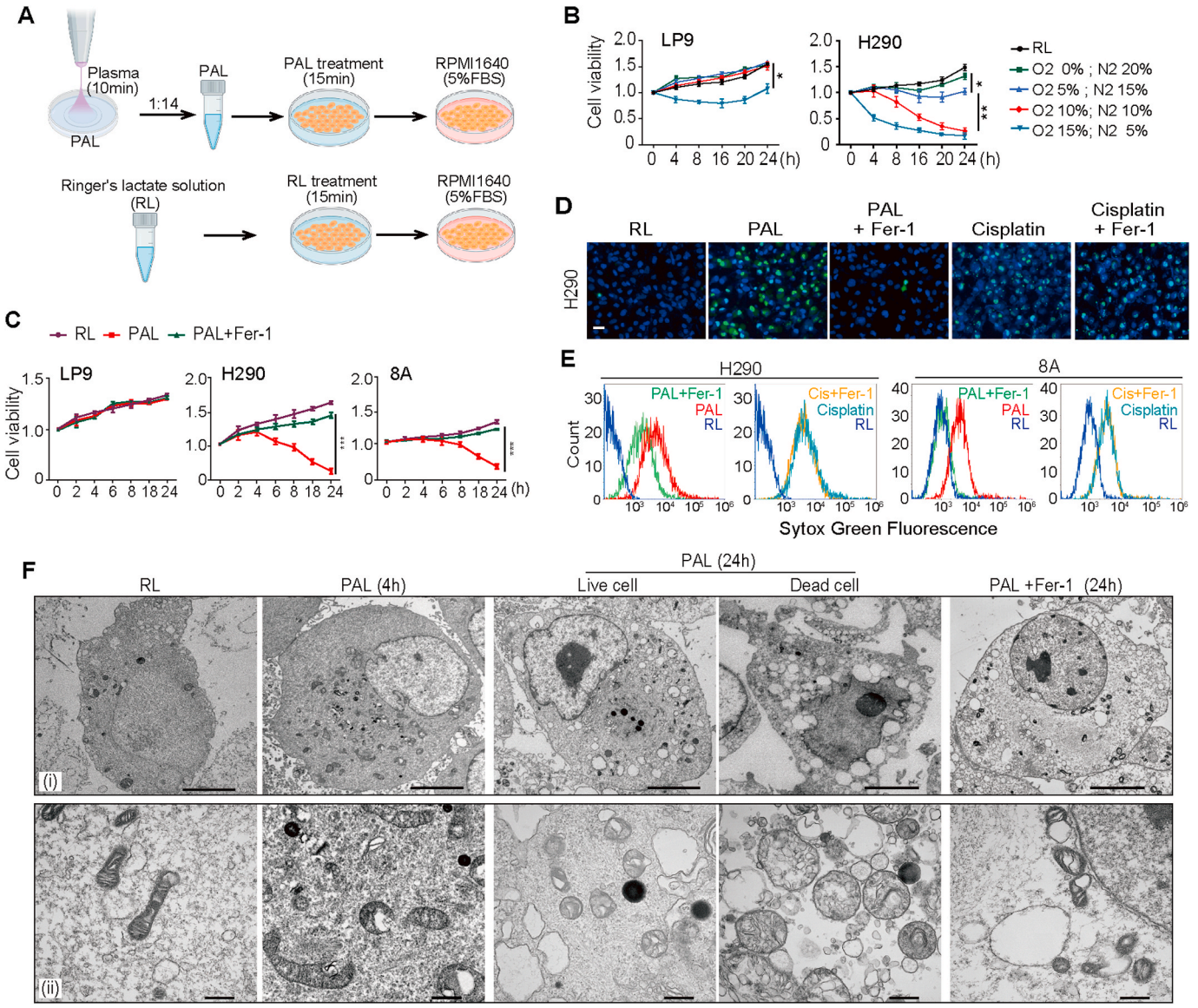

Fig. 1. *Non-thermal plasma (NTP)-activated Ringer's lactate (PAL) reveals selective, ferroptosis-inducing activity on malignant mesothelioma (MM) cells in comparison to non-tumorous mesothelial cells.* (A) Schematic illustration of experimental design. Briefly, a total of 10 mL of Ringer's lactate (RL) solution was placed in 60 mm-diameter culture dishes and exposed to NTP for 10 min, which was diluted to 14-fold with untreated Ringer's solution and used as PAL. The cells were treated with PAL for 15 min, which was further incubated in RPMI1640 medium (5% FBS). Control cells were treated with RL solution for 15 min and further incubated in RPMI1640 (5% FBS). (B) Differential effects of PAL between cancer and non-cancerous cells. Human non-tumorous mesothelial cells (LP9) and MM cells (H290, sarcomatoid subtype) were treated with PAL generated under different atmospheric composition for 15 min to evaluate cell proliferation after an incubation of 0–24 h/37 °C in RPMI (5% FBS). (C) Protective effects of Ferrostain-1 (Fer-1) only on cancer cells exposed to PAL. LP9 and MM cells (H290; 8A, epithelioid subtype) were treated with or without PAL (10% N_2/10% O_2/80% Ar) for 15 min to assess cell proliferation with or without Fer-1 (means ± SEM, N = 3; *P < 0.05, **P < 0.01, ***P < 0.001 *vs* RL unless indicated by bar). (D) PAL but not cisplatin induces ferroptosis in MM by dead cell analysis with SYTOX green and Hoechst 33342 nuclear staining under fluorescent microscopy. H290 cells were treated either with PAL (15 min), followed by an incubation of 6 h/37 °C in RPMI (5% FBS) with or without Fer-1, or with cisplatin in the presence or absence of Fer-1 for 6 h (bar = 50 μm). (E) FACS analysis of the experiments in D. Typical flow cytometry profiles are shown. (F) Transmission electron microscopy reveals (i) nuclear and (ii) mitochondrial alterations in H290 cells after PAL exposure, which are reversed by Fer-1 (bar = 5 μm at [i] and 500 nm at [ii]). Refer to text for details. (For interpretation of the references to colour in this figure legend, the reader is referred to the Web version of this article.)

with absolute factor loading values in PC1 and PC2 are shown in Supplementary Fig. 2B. Regarding 8A cells, control and PAL groups clustered significantly apart from each other by PC2. Further, Fer-1 reversed the separation between PAL and control groups. Erastin group clustered close enough with control group both by PC1 and PC2. In contrast, regarding H290 cells, PC1 differentiated control groups from PAL and erastin groups, especially with PAL group clearly dissociated. PC2 significantly separated all the five groups. PAL-group cluster showed wider distribution in comparison to that of control group. Fer-1 reversed the dissociation. Notably, there was a distinct separation between PAL and erastin groups. Supplementary Fig. 4 summarizes mapping of metabolite levels of glycolysis, pentose phosphate pathway (PPP) and tricarboxylic acid (TCA) cycle. Collectively, these results suggest that PAL exposure induces ferroptotic MM cell death, accompanied by various metabolic alterations via mechanism different from cysteine deprivation (*i.e.* erastin).

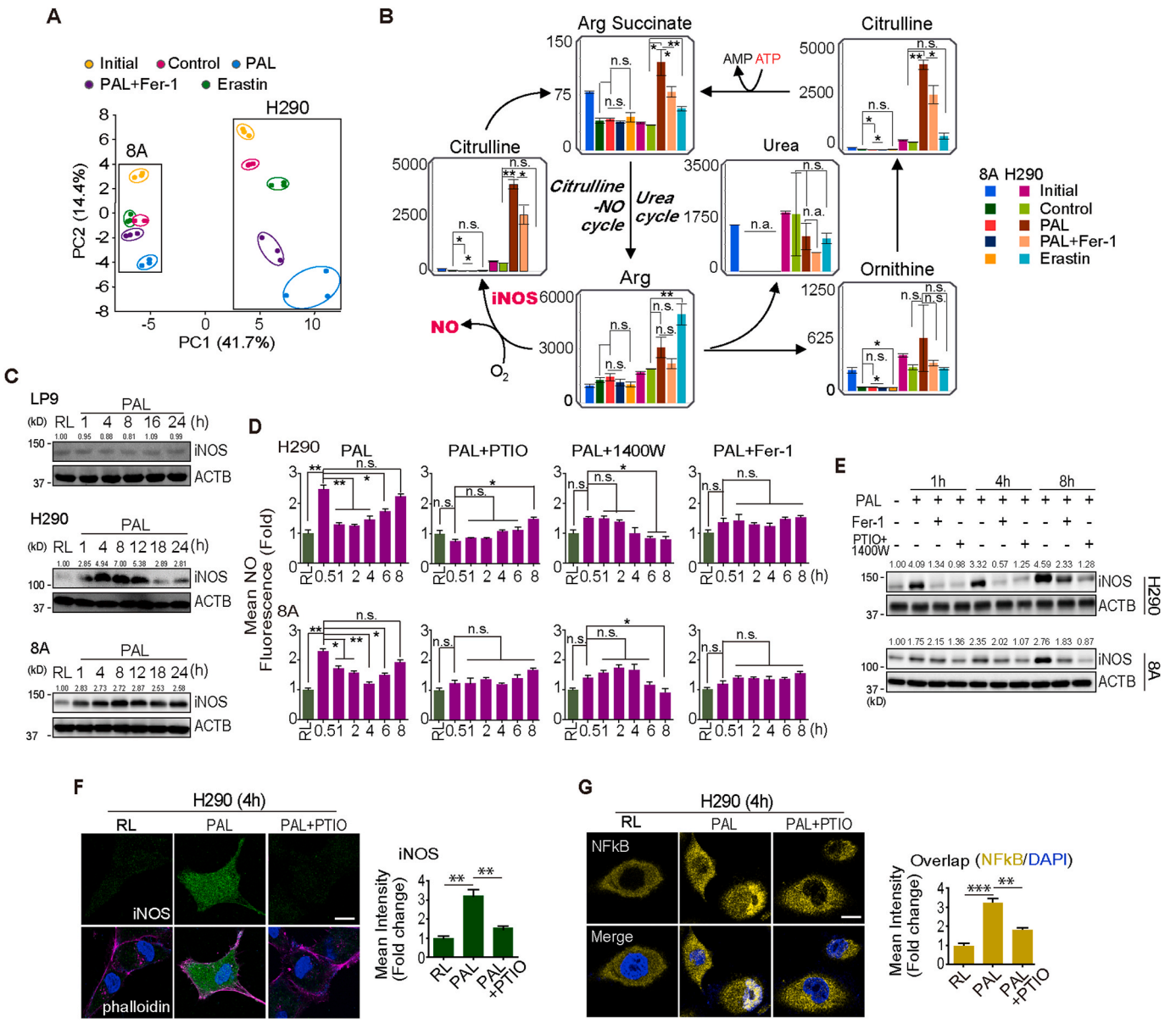

Fig. 2. *PAL effects not only through exogenous but also through endogenous nitric oxide (·NO) on MM cells.* (A) Principal components analysis (PCA) of metabolome reveals a separation of main source of variance among initial (cells cultured in complete RPMI1640 medium), control (cells cultured in RL solution), PAL treatment, PAL + Fer-1 and erastin-treatment (N = 3; H290 sarcomatoid MM; 8A, epithelioid MM). (B) Mapping of metabolite levels in citrulline-·NO cycle and urea cycle. Comparison of relative metabolite levels in cells cultivated in complete medium (initial), RL solution (control), PAL, PAL + Fer-1 or erastin. Relative metabolite levels are shown as bar plots. Characteristic reactions of citrulline-·NO cycle and urea cycle are included. (C) Specific PAL-mediated iNOS induction in MM cells. Human mesothelial cells (LP9) and MM cells (H290 and 8A) were treated with PAL (15 min) and then incubated in medium for 0–24 h/37 °C, followed by Western blot analysis. The numbers above the bands indicate relative values by quantification through the entire figures. (D) Biphasic · NO increase. MM cells were treated with or without PAL for 15 min. The cells were then incubated with or without caboxy-PTIO, 1400 W or Fer-1 for an additional 0.5–8 h/37 °C, and · NO was detected by flow cytometry using the DAF-FM DA probe. (E) Association of · NO and iNOS expression. MM cells were treated with PAL (15 min) and then incubated in medium for 0–8 h/37 °C with or without Fer-1/a combination of caboxy-PTIO and 1400 W, followed by Western blot analysis. (F) Immunofluorescence of iNOS induction after PAL exposure. H290 cells were treated with PAL (15 min) and then incubated in medium for 4 h/37 °C with or without caboxy-PTIO (DAPI nuclear staining; bar = 20 μm). (G) Immunofluorescence of NF-κB after PAL exposure. H290 cells were treated with PAL (15 min) and then incubated in medium for 4 h/37 °C with or without caboxy-PTIO (bar = 20 μm). Representative data are shown for immunofluorescence from 3 experiments and the analysis is shown as means ± SEM (N = 3), *P < 0.05, **P < 0.01, ***P < 0.001 *vs* each RL unless indicated by bar. Refer to text for details.

3.3. PAL supplies exogenous ·NO at first and later endogenous ·NO in MM cells

We recognized in the metabolome of urea cycle that levels of arginine (Arg), ornithine, citrulline and Arg succinate were all increased 4 h after PAL treatment. However, the levels of aspartate (Asp), fumaric acid, creatine and putrescine were all downregulated, which indicates that anabolism exceeded catabolism in the urea cycle (Fig. 2B; Supplementary Fig. 5). ·NO-producing cells recycle citrulline, one of the products of the NO synthase (NOS)-catalyzed reaction, to arginine in a pathway termed citrulline-·NO cycle. According to the metabolomic profiling, Fer-1 reversed the increase in the production of Arg, ornithine, citrulline and Arg succinate after PAL treatment (Fig. 2B; Supplementary Fig. 5), suggesting that PAL exposure leads to · NO production via citrulline-·NO cycle, thus contributing to ferroptosis. To confirm this hypothesis, we measured the expression of inducible NOS (iNOS [NOS2])

and the level of · NO in MM cells. An immediate increase in · NO level at 30 min and a subsequent decrease at 1 h were observed after PAL treatment (Fig. 2C and D). As PAL contains reactive oxygen and nitrogen species [38], the immediate increase in · NO level reflects the exogenous · NO from PAL. Unexpectedly, after this transient decrease, PAL caused a persistent increase in · NO level in a time-dependent manner, which was consistent with the upregulation of iNOS but neither endothelial nor neuronal NOS (eNOS [NOS3], nNOS [NOS1]; Fig. 2D; Supplementary Fig. 6D). In contrast, PAL failed to induce iNOS in human normal mesothelial cells LP9 (Fig. 2C). Furthermore, caboxy-PTIO (·NO scavenger, 100 μM), 1400 W (iNOS inhibitor, 100 μM) and Fer-1 reversed the increase in both · NO level and iNOS expression at the later phase (Fig. 2D and E). The effect of 1400 W to decrease iNOS protein level is previously described [39]. Immunocytochemistry confirmed the results (Fig. 2F; Supplementary Fig. 6B). Given that the activation of transcription factor nuclear factor (NF)-κB is a canonical mechanism to upregulate *iNOS*, we evaluated the localization of p65 and found that PAL treatment resulted in p65 translocation into the nucleus whereas · NO scavenger suppressed the activation of NF-κB (Fig. 2G; Supplementary Fig. 6C). Similarly, PAL induced cell death time-dependently in HT1080 fibrosarcoma cells with elevated level of iNOS (Supplementary Fig. 6F and G). The results demonstrate that PAL treatment provides biphasic high concentration of · NO in MM cells via NF-κB-mediated *iNOS* overexpression with a positive feedback loop.

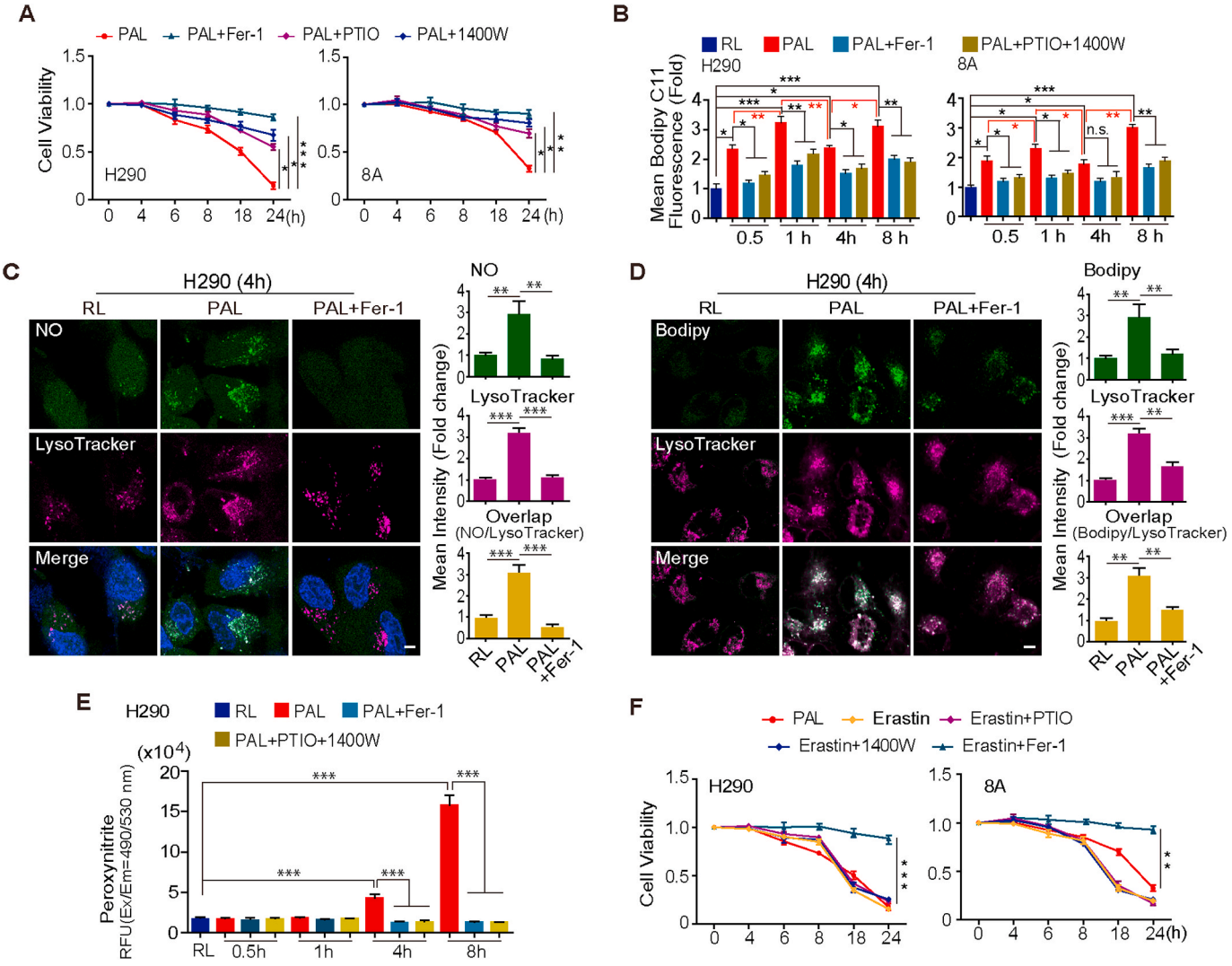

Fig. 3. *NO contributes to PAL-induced ferroptosis of MM cells* via *lysosomal localization with peroxynitrite formation.* (A) Contribution of · NO to ferroptosis evaluated by cell viability. MM cells were treated with PAL for 15 min, followed by incubation for 4–24 h with or without caboxy-PTIO, 1400 W or Fer-1 (H290, sarcomatoid MM; 8A, epithelioid MM). (B) Contribution of · NO to ferroptosis evaluated by lipid peroxidation. MM cells were treated with PAL for 15 min, followed by incubation for 0.5–8 h with or without Fer-1 or the combination of caboxy-PTIO and 1400 W, and then incubated with BODIPY™ 581/591 C11. Lipid peroxidation was evaluated by FACS analysis. (C) Lysosomal · NO after PAL exposure. After treatment with PAL (15 min) and an incubation of 4 h with or without Fer-1, H290 cells were stained with either DAF-FM DA (green) or LysoTracker Red DND-99 (red) and Hoechst 33342. The white punctate staining indicates electronic merge (Merge) of DAF-FM DA and LysoTracker by confocal microscopy (bar = 20 μm). (D) Induction of lysosomal lipid peroxidation after PAL exposure. After treatment with PAL (15 min) and an incubation of 4 h with or without Fer-1, H290 cells were stained with either BODIPY™ 581/591 C11 or LysoTracker Red DND-99 (red). The white punctate staining indicates electronic merge (Merge) of BODIPY™ 581/591 C11 and LysoTracker by confocal microscopy (bar = 20 μm). (E) Peroxynitrite production after PAL exposure. H290 cells were treated with PAL for 15 min, followed by incubation with or without Fer-1 or the combination of caboxy-PTIO and 1400 W for an additional 0.5–8 h with Peroxynitrite Sensor Green working solution. (F) Erastin-induced ferroptosis is not NO-dependent. MM cells were treated with erastin in the presence or the absence of caboxy-PTIO, 1400 W or Fer-1 for an additional 4–24 h. Cells treated with PAL for 15 min were taken as positive control. Representative data are shown from 3 experiments and the analysis is shown as means ± SEM (N = 3), *P < 0.05, **P < 0.01, ***P < 0.001 *vs* each RL unless indicated by bar. (For interpretation of the references to colour in this figure legend, the reader is referred to the Web version of this article.)

3.4. ·NO plays a major role in PAL-induced ferroptosis

To determine the role of · NO in PAL-induced ferroptosis, we evaluated whether · NO scavenger and iNOS inhibitor affect PAL-induced ferroptosis of MM cells. Caboxy-PTIO and 1400 W significantly reversed PAL-induced ferroptosis (Fig. 3A; Supplementary Fig. 6A). Moreover, increased lipid peroxidation by PAL exposure was inhibited by Fer-1 or by the combination of Caboxy-PTIO and 1400 W (for the elimination of exogenous and endogenous · NO) (Fig. 3B). To analyze how · NO eventually contributed to lipid peroxidation, we screened for the localization of · NO and lipid peroxidation with specific probes. In PAL-treated MM cells, the accumulation of · NO and lipid peroxidation was unexpectedly both at lysosomes, which Fer-1 could protect from undergoing this · NO-derived oxidants-mediated lipid peroxidation (Fig. 3C and D; Supplementary Fig. 7A, B). Given that peroxynitrite is generated by the combination of · NO and O_2^- and plays a critical role in pro-oxidation [40], we determined the level of peroxynitrite in PAL-treated MM cells. A time-dependent increase in peroxynitrite was observed upon PAL treatment, which was reversed by Fer-1 or by the combination of caboxy-PTIO and 1400 W (Fig. 3E; Supplementary Fig. 7C). The observation suggests not only the unexpected role of · NO but also of lysosome in PAL-induced ferroptosis in MM cells. Of note, we found that cysteine deprivation-derived ferroptosis by erastin leads to a significantly different metabolic alterations in citrulline-·NO cycle (Fig. 2A), suggesting a different mechanism of ferroptosis. As expected, neither caboxy-PTIO nor 1400 W could reverse erastin-induced ferroptosis (Fig. 3E), confirming that PAL-induced ferroptosis is unique in nature.

3.5. ·NO induces lysosome-dependent autophagy at the early phase after PAL exposure

In addition to the activation of citrulline-·NO cycle, metabolome analysis revealed another category of results that levels of essential amino acids (AAs) are significantly increased in PAL-treated group despite AA deficiency in the culture media. Regarding H290 cell line, amounts of 8 out of 9 essential AAs (His, Ile, Leu, Thr, Phe, Lys, Trp and Val) were increased in response to PAL treatment whereas Fer-1 reversed the enhancement of 5 AAs (His, Ile, Leu, Thr, and Val) (Fig. 4A). Moreover, PAL-treated cells exhibited a significant increase in the number of phagophore, lysosomes and autolysosomes (Fig. 4B). The observation led to a hypothesis that at this stage (4 h after PAL treatment) MM cells undergo the autophagic process, especially in lysosomes, in response to accumulation of lipid peroxidation.

Indeed, we found that PAL treatment increased the expression of LC3B-II in a time-dependent manner whereas Fer-1 or the combination of PTIO and 1400 W reversed the increase (Fig. 4C and D; Supplementary Fig. 8A). Moreover, redistribution of LC3B from the nucleus, as described in cancer cell lines [41], to the cytoplasm also suggested the induction of autophagy in PAL-treated cells (Fig. 4C). Lysosomal membrane marker, LAMP1, was similarly increased but decreased 8 h after PAL treatment in comparison to 4 h, suggesting the temporary induction of lysosomal biogenesis with autophagy [42], followed by extensive lysosomal damage (Fig. 4D). To gain a better insight into how lysosomes participate in this process, we used bafilomycin A1 (10 nM) [29], which prevents maturation of autophagic vacuoles by inhibiting late-stage fusion between autophagosomes and lysosomes as well as lysosomal degradation (Fig. 4F). Bafilomycin A1 protected MM cells from PAL-induced ferroptosis via maintaining lysosomal function (Fig. 4E and F). Moreover, bafilomycin A1 eliminated NO accumulation and lipid peroxidation in lysosomes (Fig. 4G and H; Supplementary Fig. 8B, C). Taken together, these results indicate that PAL induces and also requires autophagic process as an early event to cause · NO-derived oxidants-mediated lipid peroxidation in lysosomes. The pH of lysosome is estimated as ~5. ·NO probe is stable above pH 5.8 and would be ~90% at pH 5 [35], and C11-BODYPY for lipid peroxidation is stable at all pH [37], confirming these experiments are reasonable.

3.6. P62-regulated lipid peroxidation leads to ferroptosis at the late phase after PAL exposure

mTORC1 represses autophagy by directly inhibiting specific Atg proteins required for autophagy induction [43]. Further, mTORC1 is able to control transcription factor EB (TFEB) activation by maintaining it in the cytosol [44]. However, upon stimulation, such as fasting, TFEB rapidly translocates to the nucleus, inducing expression of autophagy and lysosomal genes, including p62, a multifunctional signaling hub protein [45]. We evaluated the subcellular localization of TFEB and the expression of phosphorylated mTOR (pmTOR) and p62. p62 was persistently overexpressed for 8 h after PAL exposure whereas pmTOR decreased 4 and 8 h after PAL treatment in H290 and 8A cells, respectively. Notably, Fer-1 or the combination of caboxy-PTIO and 1400 W could reverse both of them (Fig. 5A). PAL induced an increase in the nuclear TFEB whereas bafilomycin A1 or the combination of caboxy-PTIO and 1400 W could prevent it (Fig. 5B; Supplementary Fig. 9A).

Here downregulation of pmTORC1 activated TFEB, which resulted in the transcription of p62, initiating autophagy, at the early phase after PAL exposure. p62 levels thereafter increased up to 8 h, followed by gradual decrease as a function of time until 24 h, when p62 level was lower than that at 0 h, concomitant with the increase in pmTOR levels (Fig. 5C and D; Supplementary Fig. 9B). The results, together with the rapidly decreasing LC3B and Keap1 levels after 8 h with similar time-course, indicate the inhibition of autophagy (Fig. 5D). As p62/Keap1/Nrf2 plays an important role in mediating oxidative stress response [46], we then examined the oxidative stress levels by lipid peroxidation and peroxides. As mentioned above, oxidative stress rapidly and significantly increased 1 h after PAL treatment, followed by a temporary decrease at 4 h, which may be due to the regulatory activity of p62-mediated antioxidant response (Fig. 5E and F). After 4 h, oxidative stress level then gradually increased until 24 h with the decrease in p62 and Keap1 levels (Fig. 5D, E and F) and the nuclear translocation of Nrf2 (Supplementary Fig. 9C). Moreover, bafilomycin A1 reversed the elevated level of p62 induced by PAL (Supplementary Fig. 9D, E), indicating that its eliminating effect of lipid ROS (Fig. 4H) might be partly due to the regulation of p62. This observation was consistent with the fate of ferroptosis, suggesting that ferroptosis signal has a higher hierarchy than the pro-autophagic response as the late-phase event after PAL exposure.

4. Discussion

NTP technology, an engineered source of various reactive species, has long been used in industry to remove · NO and SO_2 in the gas phase in combination with TiO_2 photocatalytst [47]. Here we for the first time revealed that PAL, a simple solution after NTP exposure, causes ferroptosis in a lysosomal · NO-dependent manner specifically in cancer (MM) cells.

Cancer cells are generally rich in catalytic Fe(II) for frequent DNA replication and persistent proliferation, which can be the Achilles' heel targets to induce ferroptosis specifically [3,48]. PAL-mediated ferroptosis was different in metabolic and signaling processes from that of erastin, a classic cysteine deprivation-type ferroptosis inducer, based on the present metabolomic study. We evaluated alterations in intracellular metabolites in PAL-treated MM cells, which were compared to those of PAL/Fer-1- and erastin-treated MM cells. We could identify upregulation of citrulline-·NO cycle by PAL exposure, but not by erastin. Of note, this upregulation was inhibited by Fer-1, indicating a distinct ferroptosis pathway. ·NO is involved in various aspects of physiological and pathological processes in biology [40,49,50]. Citrulline in human blood is increased with aging [51]. Regulation of iNOS with · NO production is complex and still controversial especially in cancer [39,52–54]. Biphasic

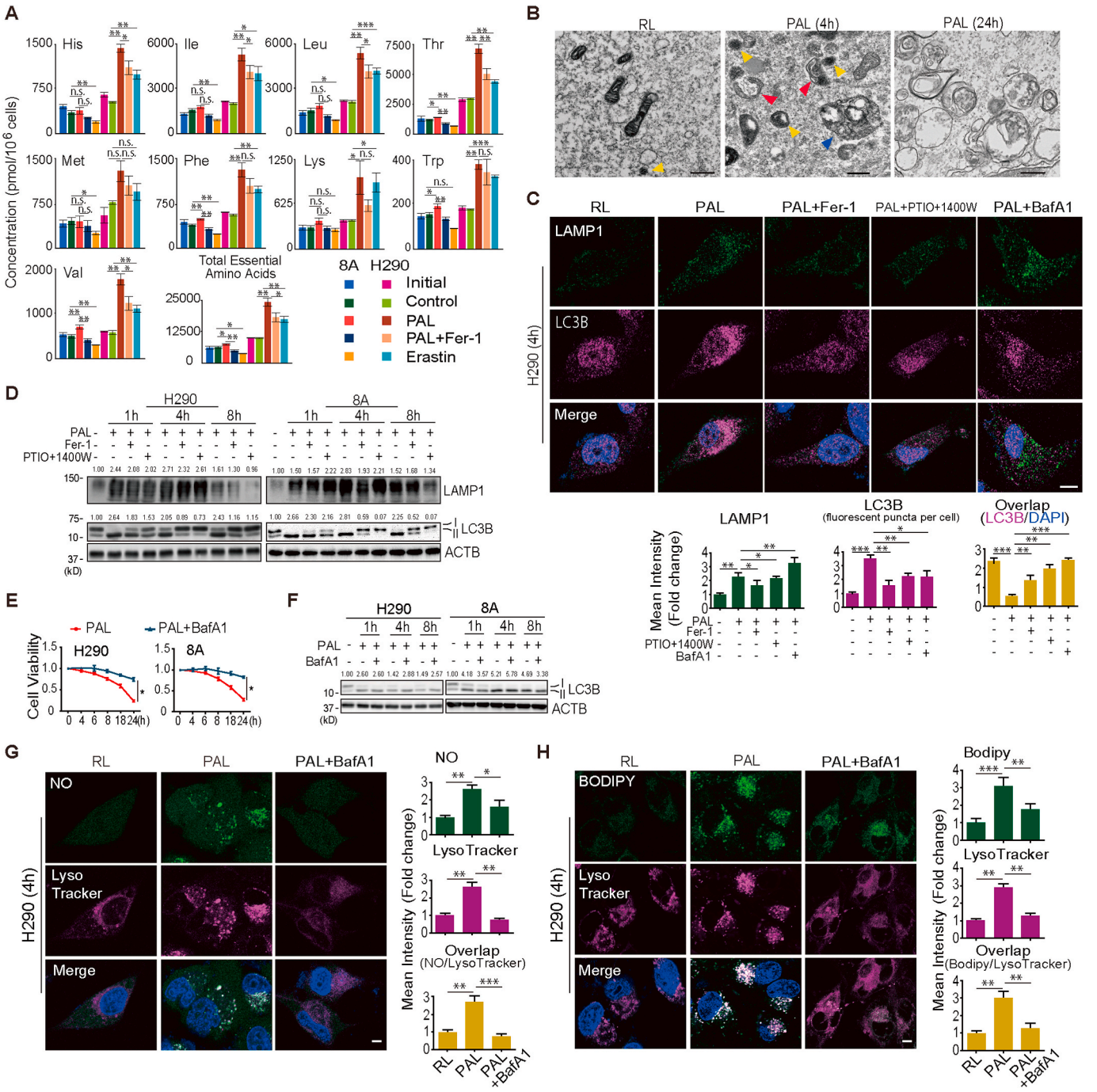

Fig. 4. *PAL initiates lysosome-dependent autophagy in MM cells.* (A) Essential amino acids in MM cells cultured in RPMI (initial), Ringer's solution (control), PAL, PAL with Fer-1 or erastin. Relative metabolite levels shown as bar plots. (B) Autophagy by transmission electron microscopy of H290 cells treated with PAL. Red, blue and yellow arrowheads represent phagophore, autolysosome and lysosome, respectively (bar = 500 nm). (C) Proximity of LAMP1 to LC3B after PAL. H290 cells were treated with PAL, followed by 4-h incubation with or without Fer-1, the combination of caboxy-PTIO and 1400 W, or bafilomycin A1 (BafA1), and immunostained with anti-LAMP1 and anti-LC3B antibodies (Hoechst 33342) evaluated by confocal microscopy (bar = 20 μm). (D) Initiation of autophagy with lysosomegenesis after PAL. MM cells were treated with PAL for 15 min, followed by incubation with or without Fer-1 or the combination of caboxy-PTIO and 1400 W for 1–8 h, and the expression of LAMP1 and LC3B were assessed by Western blot. (E) Autophagic process is necessary for PAL-induced ferroptosis. MM cells were treated with PAL for 15 min, which was followed by incubation with or without bafilomycin A1 for 4–24 h. (F) MM cells were treated with PAL for 15 min. The cells were then incubated with or without bafilomycin A1 for an additional 1–8 h, and the expression of LC3B were assessed by Western blot. (G) Autophagic process is necessary for PAL-induced lysosomal · NO accumulation. After PAL treatment (15 min) and 4-h incubation with or without bafilomycin A1, H290 cells were stained either with DAF-FM DA (green) or LysoTracker Red DND-99 (red; Hoechst 33342). Merge (white) of DAF-FM DA and LysoTracker by confocal microscopy (bar = 20 μm). (H) Autophagic process is necessary for PAL-induced lysosomal lipid peroxidation. After treatment with PAL (15 min) and an incubation of 4 h with or without bafilomycin A1, H290 cells were stained either with BODIPY™ 581/591 C11 or LysoTracker Red DND-99 (red; 10 μM) evaluated by confocal microscopy (bar = 20 μm). Representative data are shown from 3 experiments and the analysis is shown as means ± SEM (N = 3), *P < 0.05, **P < 0.01, ***P < 0.001 *vs* each RL unless indicated by bar. (For interpretation of the references to colour in this figure legend, the reader is referred to the Web version of this article.)

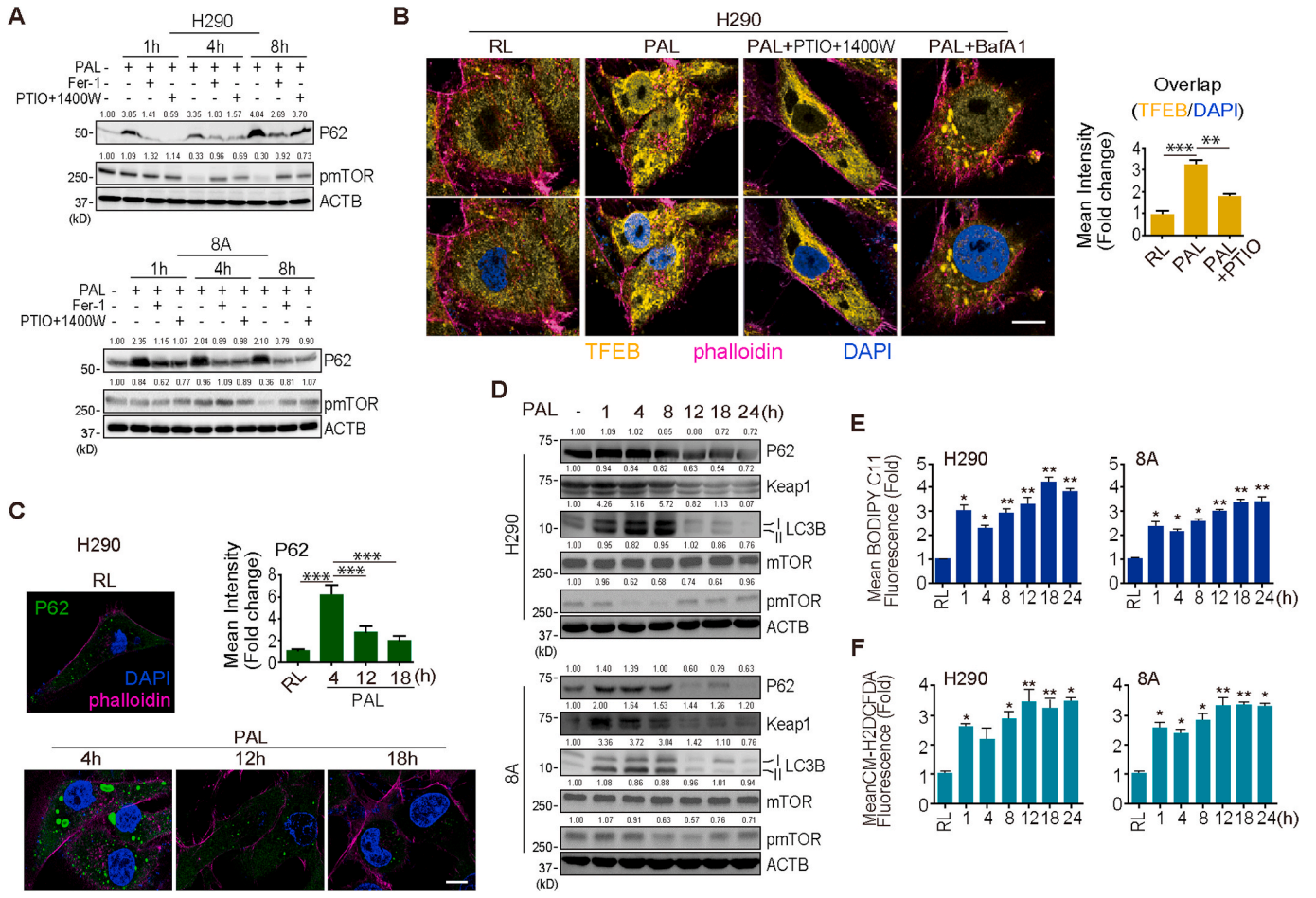

Fig. 5. *Failure of phophorylated mTOR/TFEB/p62 signaling leads to ferroptosis of MM cells after PAL.* (A) pmTOR reduction with p62 induction at an early phase after PAL exposure. MM cells were treated with PAL for 15 min. The cells were then incubated with or without Fer-1 or the combination of caboxy-PTIO and 1400 W for an additional 1–8 h, and the expression of p62 and pmTOR were assessed by Western blot. (B) TFEB induction is associated with · NO and autophagic processes. H290 cells were treated with or without PAL, and then incubated for an additional 4 h in the presence or the absence of the combination of caboxy-PTIO and 1400 W or bafilomycin A1. Immunocytochemistry was performed with anti-TEFB antibody (lower panel, DAPI nuclear staining), which was observed using confocal microscopy (bar = 20 μm). (C) Early increase and late decrease of p62 in MM cells after PAL. H290 cells were treated with PAL, and then incubated for an additional 4–18 h. Immunocytochemistry was with anti-p62 antibody, which was observed using confocal microscopy (bar = 20 μm). (D) Time course of pmTOR/p62/LC3B. MM cells were treated with or without PAL for 15 min. The cells were then incubated for an additional 1–24 h, and the expression of p62, Keap1, LC3B, mTOR, pmTOR was assessed by Western blot. (E) Increase in lipid peroxidation after PAL. After treatment with PAL (15 min) and an incubation of 1–24 h, the cells were stained for 30 min/37 °C with BODIPY™ 581/591 C11. The level of lipid peroxidation was examined by FACS analysis. (F) After treatment with PAL (15 min) and an incubation of 1–24 h, the cells were stained for 30 min/37 °C with CM-H2DCFDA. The level of ROS was examined by FACS analysis. Representative data are shown from 3 experiments and the analysis is shown as means ± SEM (N = 3), *P < 0.05, **P < 0.01, ***P < 0.001 *vs* each RL unless indicated by bar.

contribution of · NO to ferroptosis was unexpected, and our observation supports a role of exogenous · NO in the amplification of iNOS-derived · NO levels in MM cells with a positive feedback loop through NF-κB activation (Fig. 6A).

Lysosomes in MM cells were the critical subcellular location for the effects of PAL. Cancer cells are rich in lysosome [55], which harbors abundant catalytic Fe(II) and is a key organelle for iron homeostasis under cell proliferation [56]. ·NO has strong affinity for Fe(II) and O_2^- may be coexistent via lysosomal membrane-associated NADPH oxidase [57]. The reaction of · NO with O_2^- leads to pro-oxidant events with the intermediacy of peroxynitrite, including lipid peroxidation of poly-unsaturated fatty acids present in biomembranes and lipoproteins [40]. Here we showed for the first time that · NO-derived oxidants-mediated lipid peroxidation in the execution of ferroptosis in MM cells, which was distinct from a previous report in PAL-treated A549 lung adenocarcinoma cells, where mitochondria were the major target and NF-κB was downregulated [58]. Thus, histology- or origin-specificity of cancer may be present for the effects of PAL, necessitating further investigation. Our results provide with a novel insight of · NO in the regulation of ferroptosis where · NO donors may promote the effect of chemotherapy, especially in MM of sarcomatoid subtype.

Oxidative stress plays a role in regulating the balance between cell survival and death, making it a double-edged sword in cancer progression and therapy [59]. During the way toward ferroptosis in PAL-exposed MM cells, we observed autophagic process at an early phase with · NO accumulation and lipid peroxidation in lysosomes. We believe that this autophagy is a protective process, supported by the observation of temporary decrease in lipid peroxidation level (4 h), which was followed by significant upregulation of lysosomal biosynthesis and p62 transcription. Multifunctional protein p62 not only acts as an autophagy substrate protein, but also participates in antioxidant response by activating Keap1/Nrf2 pathway [46], which may provide with another explanation for the protective response at this timepoint.

However, pro-survival phase of autophagy was transformed into ferroptosis past a threshold, when significant ferroptosis was observed 12 h after PAL exposure. This was accompanied by a rapid decrease in lysosomal biosynthesis, p62 expression and LC3B levels with increasing lipid peroxidation. We believe, based on our results, that this switching

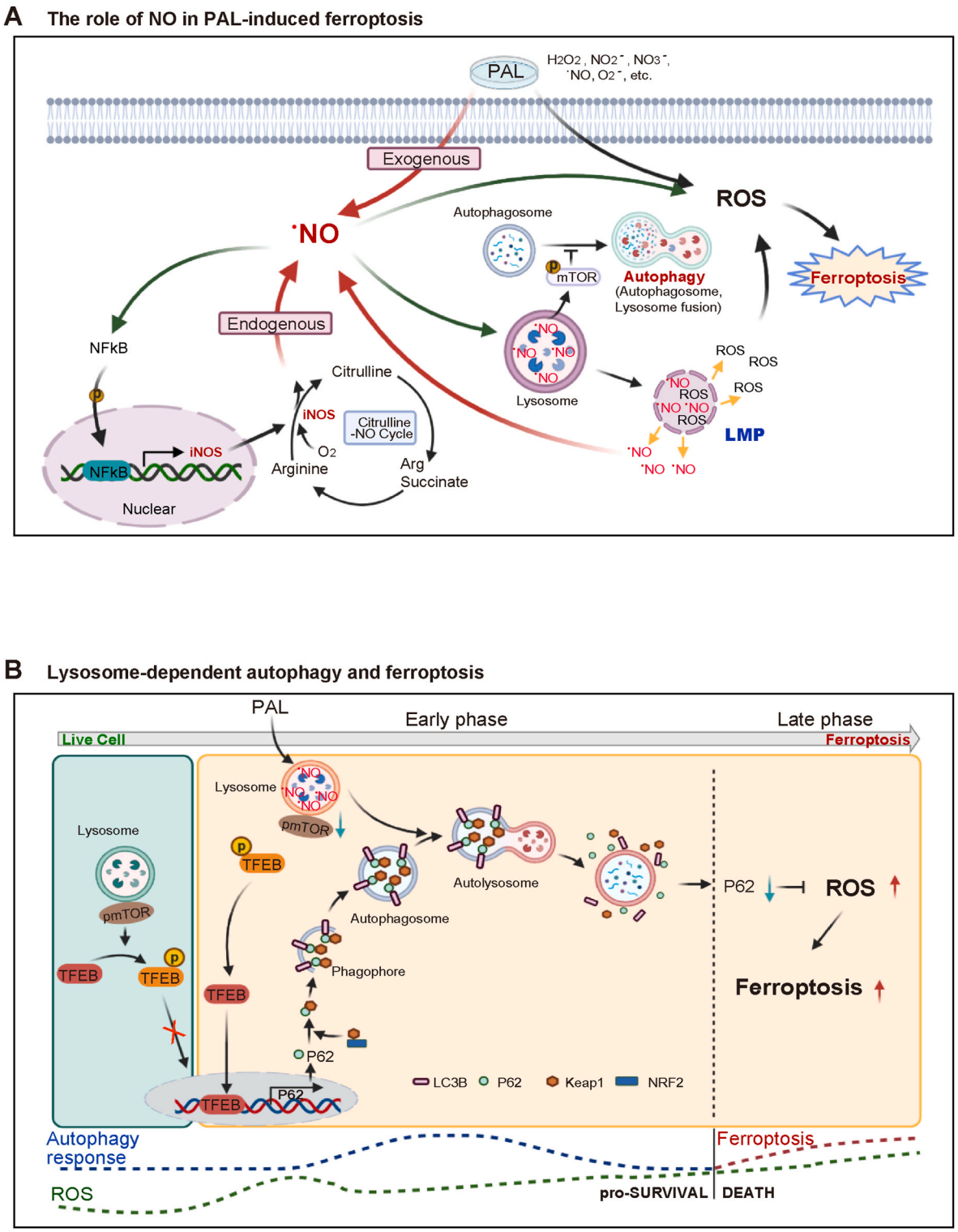

Fig. 6. (A) *Role of · NO in PAL-induced ferroptosis in MM cells.* PAL provides MM cells with an immediate impact of exogenous · NO, a component of PAL. The initial stimulation of · NO activates transcription factor NF-κB in MM cells, upregulating the downstream iNOS as revealed by metabolome analysis. In return, this positive feedback loop leads to sustained accumulation of · NO in lysosomes. Simultaneously, ·NO accumulation in lysosomes starts autophagic process, eventually resulting in lysosomal membrane permeabilization (LMP) upon certain threshold according with increase in lysosomal lipid peroxidation. The whole process eventually leads to ferroptosis. (B) *Molecular switch from autophagy to ferroptosis in MM cells.* In the absence of PAL stress, mTOR binds to *p*-TFEB, which keeps the autophagy event in a physiological level. Under PAL exposure, MM cells, by responding to exogenous reactive species, start autophagic processes, initialized by translocation of TFEB into the nucleus and the subsequent upregulation of *p62* transcription. During this early event, autophagy serves as a survival mechanism and the following p62-Keap1–Nrf2 axis-mediated antioxidant response would keep the balance of ROS for a period of time. However, sustained accumulation of · NO-derived oxidants-mediated lipid peroxidation, and lysosomal dysfunction eventually results in ferroptosis, when autophagic process is terminated. The molecular switching of cell fate from autophagy for survival to ferroptosis occurs when autophagic proteins, such as p62, are downregulated as a consequence of accumulated lipid peroxidation in lysosomes.

contains the following molecular events; 1) lysosomal function and biogenesis were suppressed at the late phase of PAL exposure, indicating loss of lysosomal activity to maintain homeostasis (failure of lysophagy [60] and iron homeostasis [56]); 2) lysosomal damage may be an essential reason for the cells to cease autophagic process; 3) lysosomal membrane damage results in the release of catalytic Fe(II), lysosomal enzymes and reactive species into the cytosol, thus executing cell death; 4) sustained lipid peroxidation leads to the downregulation or damage of p62 at the late phase, which may result in the dysfunction of p62/Keap1/Nrf2-mediated antioxidant response, leading to a further accelerated accumulation of lipid peroxidation, and thus constitutes a switch from autophagy into ferroptosis (Fig. 6B). Other possibilities of the associated molecular mechanisms include 5) oxidative DNA damage of promoter regions in autophagy-associated genes, including *p62*, is significant enough to inhibit autophagy [61]; 6) autophagy-associated proteins may subject to redox-specific post-translational modifications at Cys residues, which may determine their role as pro-survival *versus* pro-death [62], which require further studies.

Of note, it was recently reported that obesity promotes hepatic lysosomal iNOS localization and subsequent overproduction of lysosomal · NO, which contributes to hepatic insulin-resistance in obese mice [63]. We believe that hepatic lysosomal iNOS induction of this case is similar in mechanisms but in a milder fashion in pathology.

In conclusion, we demonstrated for the first time that PAL induces ferroptosis in MM cells via lysosomal · NO-derived oxidants-mediated lipid peroxidation. Our results point to an important scenario that · NO is a potential regulator of ferroptosis through autophagic processes, which may be interpreted as lysophagy failure. Moreover, the presence of a threshold from the early autophagic phase into the late ferroptotic phase elicited by PAL exposure provides us with a novel understanding toward oxidative stress-dependent cancer therapies. PAL can be a burgeoning ferroptosis-directed cancer therapy, flexibly combined with other modalities.

Author contributions

LJ, HZ, KN, HT, KI, HK, MM, MH and ST contributed to the conception and design of the work. LJ, HZ, QL, SH, KS and KN contributed to the acquisition of the data. LJ, HZ, YS, KN, HT, MM and ST analyzed and interpreted the data. LJ and HZ drafted the work and ST substantially revised it.

Declaration of competing interest

All the authors declare no conflict of interest.

Acknowledgements

This work was supported, in part, by JSPS Kakenhi (Grant Number JP17H04064, JP19H05462 and JP20H05502) and Research Grant of the Princess Takamatsu Cancer Research Fund (19–251) to ST. Electron microscopic analyses were supported by Koji Itakura, Division of Medical Research Engineering, Nagoya University Graduate School of Medicine. We thank Prof. Rafael Radi (Universidad de la República, Uruguay) for critical comments.

Appendix A. Supplementary data

Supplementary data to this article can be found online at https://doi.org/10.1016/j.redox.2021.101989.

References

[1] S. Toyokuni, Y. Kong, Z. Cheng, K. Sato, S. Hayashi, F. Ito, L. Jiang, I. Yanatori, Y. Okazaki, S. Akatsuka, Carcinogenesis as side effects of iron and oxygen utilization: from the unveiled truth toward ultimate bioengineering, Cancers 12 (11) (2020) 3320.

[2] Y. Zhang, J. Shi, X. Liu, L. Feng, Z. Gong, P. Koppula, K. Sirohi, X. Li, Y. Wei, H. Lee, L. Zhuang, G. Chen, Z.D. Xiao, M.C. Hung, J. Chen, P. Huang, W. Li, B. Gan, BAP1 links metabolic regulation of ferroptosis to tumour suppression, Nat. Cell Biol. 20 (10) (2018) 1181–1192.

[3] S. Toyokuni, I. Yanatori, Y. Kong, H. Zheng, Y. Motooka, L. Jiang, Ferroptosis at the crossroads of infection, aging and cancer, Canc. Sci. 111 (2020) 2665–2671.

[4] F. Ito, T. Nishiyama, L. Shi, M. Mori, T. Hirayama, H. Nagasawa, H. Yasui, S. Toyokuni, Contrasting intra- and extracellular distribution of catalytic ferrous iron in ovalbumin-induced peritonitis, Biochem. Biophys. Res. Commun. 476 (4) (2016) 600–606.

[5] J.D. Schoenfeld, Z.A. Sibenaller, K.A. Mapuskar, B.A. Wagner, K.L. Cramer-Morales, M. Furqan, S. Sandhu, T.L. Carlisle, M.C. Smith, T. Abu Hejleh, D.J. Berg, J. Zhang, J. Keech, K.R. Parekh, S. Bhatia, V. Monga, K.L. Bodeker, L. Ahmann, S. Vollstedt, H. Brown, E.P. Shanahan Kauffman, M.E. Schall, R.J. Hohl, G. H. Clamon, J.D. Greenlee, M.A. Howard, M.K. Schultz, B.J. Smith, D.P. Riley, F. E. Domann, J.J. Cullen, G.R. Buettner, J.M. Buatti, D.R. Spitz, B.G. Allen, O2(-) and H_2O_2-mediated disruption of Fe metabolism causes the differential susceptibility of NSCLC and GBM cancer cells to pharmacological ascorbate, Canc. Cell 31 (4) (2017) 487–500 e8.

[6] B.R. Stockwell, J.P. Friedmann Angeli, H. Bayir, A.I. Bush, M. Conrad, S.J. Dixon, S. Fulda, S. Gascon, S.K. Hatzios, V.E. Kagan, K. Noel, X. Jiang, A. Linkermann, M. E. Murphy, M. Overholtzer, A. Oyagi, G.C. Pagnussat, J. Park, Q. Ran, C. S. Rosenfeld, K. Salnikow, D. Tang, F.M. Torti, S.V. Torti, S. Toyokuni, K. A. Woerpel, D.D. Zhang, Ferroptosis: a regulated cell death nexus linking metabolism, Redox Biology, and Disease, Cell 171 (2) (2017) 273–285.

[7] B. Proneth, M. Conrad, Ferroptosis and necroinflammation, a yet poorly explored link, Cell Death Differ. 26 (1) (2019) 14–24.

[8] B. Wiernicki, H. Dubois, Y.Y. Tyurina, B. Hassannia, H. Bayir, V.E. Kagan, P. Vandenabeele, A. Wullaert, T. Vanden Berghe, Excessive phospholipid peroxidation distinguishes ferroptosis from other cell death modes including pyroptosis, Cell Death Dis. 11 (10) (2020) 922.

[9] T. Xu, W. Ding, X. Ji, X. Ao, Y. Liu, W. Yu, J. Wang, Molecular mechanisms of ferroptosis and its role in cancer therapy, J. Cell Mol. Med. 23 (8) (2019) 4900–4912.

[10] J.P.F. Angeli, D.V. Krysko, M. Conrad, Ferroptosis at the crossroads of cancer-acquired drug resistance and immune evasion, Nat. Rev. Canc. 19 (7) (2019) 405–414.

[11] Y.Q. Wu, S.W. Zhang, X.X. Gong, S. Tam, D.S. Xiao, S. Liu, Y.G. Tao, The epigenetic regulators and metabolic changes in ferroptosis-associated cancer progression, Mol. Canc. 19 (1) (2020) 39.

[12] IARC, WHO, Asbestos (chrysotile, amosite, crocidolite, tremolite, actinolite, and anthophyllite), in: IARC Monographs on the Evaluation of Carcinogenic Risks to Humans. A Review of Human Carcinogens; Part C: Arsenic, Metals, Fibres, and Dusts, Lyon, France, 2012, pp. 219–309.

[13] L. Jiang, S. Akatsuka, H. Nagai, S.H. Chew, H. Ohara, Y. Okazaki, Y. Yamashita, Y. Yoshikawa, H. Yasui, K. Ikuta, K. Sasaki, Y. Kohgo, S. Hirano, Y. Shinohara, N. Kohyama, T. Takahashi, S. Toyokuni, Iron overload signature in chrysotile-induced malignant mesothelioma, J. Pathol. 228 (2012) 366–377.

[14] S. Toyokuni, Iron addiction with ferroptosis-resistance in asbestos-induced mesothelial carcinogenesis: toward the era of mesothelioma prevention, Free Radic. Biol. Med. 133 (2019) 206–215.

[15] A. Reid, N.H. de Klerk, C. Magnani, D. Ferrante, G. Berry, A.W. Musk, E. Merler, Mesothelioma risk after 40 years since first exposure to asbestos: a pooled analysis, Thorax 69 (9) (2014) 843–850.

[16] J.L. Beebe-Dimmer, J.P. Fryzek, C.L. Yee, T.B. Dalvi, D.H. Garabrant, A. G. Schwartz, S. Gadgeel, Mesothelioma in the United States: a surveillance, epidemiology, and end results (SEER)–Medicare investigation of treatment patterns and overall survival, Clin. Epidemiol. 8 (2016) 743.

[17] S. Kalghatgi, C.M. Kelly, E. Cerchar, B. Torabi, O. Alekseev, A. Fridman, G. Friedman, J. Azizkhan-Clifford, Effects of non-thermal plasma on mammalian cells, PloS One 6 (1) (2011), e16270.

[18] Y. Okazaki, Y. Wang, H. Tanaka, M. Mizuno, K. Nakamura, H. Kajiyama, H. Kano, K. Uchida, F. Kikkawa, M. Hori, S. Toyokuni, Direct exposure of non-equilibrium atmospheric pressure plasma confers simultaneous oxidative and ultraviolet modifications in biomolecules, J. Clin. Biochem. Nutr. 55 (3) (2014) 207–215.

[19] H. Tanaka, M. Mizuno, S. Toyokuni, S. Maruyama, Y. Kodera, H. Terasaki, T. Adachi, M. Kato, F. Kikkawa, M. Hori, Cancer therapy using non-thermal atmospheric pressure plasma with ultra-high electron density, Phys. Plasmas 22 (12) (2015) 122004.

[20] H. Kajiyama, F. Utsumi, K. Nakamura, H. Tanaka, S. Toyokuni, M. Hori, F. Kikkawa, Future perspective of strategic non-thermal plasma therapy for cancer treatment, J. Clin. Biochem. Nutr. 60 (1) (2017) 33–38.

[21] S. Toyokuni, Y. Ikehara, F. Kikkawa, M. Hori, Plasma Medical Science, Academic Press, 2018.

[22] L. Shi, Y. Wang, F. Ito, Y. Okazaki, H. Tanaka, M. Mizuno, M. Hori, D. R. Richardson, S. Toyokuni, Biphasic effects of l-ascorbate on the tumoricidal activity of non-thermal plasma against malignant mesothelioma cells, Arch. Biochem. Biophys. 605 (2016) 109–116.

[23] L. Shi, F. Ito, Y. Wang, Y. Okazaki, H. Tanaka, M. Mizuno, M. Hori, T. Hirayama, H. Nagasawa, D.R. Richardson, S. Toyokuni, Non-thermal plasma induces a stress response in mesothelioma cells resulting in increased endocytosis, lysosome biogenesis and autophagy, Free Radic. Biol. Med. 108 (2017) 904–917.

[24] P. Darvin, S.M. Toor, V. Sasidharan Nair, E. Elkord, Immune checkpoint inhibitors: recent progress and potential biomarkers, Exp. Mol. Med. 50 (12) (2018) 1–11.

[25] N. Usami, T. Fukui, M. Kondo, T. Taniguchi, T. Yokoyama, S. Mori, K. Yokoi, Y. Horio, K. Shimokata, Y. Sekido, T. Hida, Establishment and characterization of

four malignant pleural mesothelioma cell lines from Japanese patients, Canc. Sci. 97 (5) (2006) 387–394.
[26] S.J. Dixon, K.M. Lemberg, M.R. Lamprecht, R. Skouta, E.M. Zaitsev, C.E. Gleason, D.N. Patel, A.J. Bauer, A.M. Cantley, W.S. Yang, Ferroptosis: an iron-dependent form of nonapoptotic cell death, Cell 149 (5) (2012) 1060–1072.
[27] T. Akaike, M. Yoshida, Y. Miyamoto, K. Sato, M. Kohno, K. Sasamoto, K. Miyazaki, S. Ueda, H. Maeda, Antagonistic action of imidazolineoxyl N-oxides against endothelium-derived relaxing factor/.NO through a radical reaction, Biochemistry 32 (3) (1993) 827–832.
[28] E.P. Garvey, J.A. Oplinger, E.S. Furfine, R.J. Kiff, F. Laszlo, B.J. Whittle, R. G. Knowles, 1400W is a slow, tight binding, and highly selective inhibitor of inducible nitric-oxide synthase in vitro and in vivo, J. Biol. Chem. 272 (8) (1997) 4959–4963.
[29] H. Tapper, R. Sundler, Bafilomycin A1 inhibits lysosomal, phagosomal, and plasma membrane H(+)-ATPase and induces lysosomal enzyme secretion in macrophages, J. Cell. Physiol. 163 (1) (1995) 137–144.
[30] H. Tanaka, M. Mizuno, Y. Katsumata, K. Ishikawa, H. Kondo, H. Hashizume, Y. Okazaki, S. Toyokuni, K. Nakamura, N. Yoshikawa, H. Kajiyama, F. Kikkawa, M. Hori, Oxidative stress-dependent and -independent death of glioblastoma cells induced by non-thermal plasma-exposed solutions, Sci. Rep. 9 (1) (2019) 13657.
[31] K. Ishikawa, Y. Hosoi, H. Tanaka, L. Jiang, S. Toyokuni, K. Nakamura, H. Kajiyama, F. Kikkawa, M. Mizuno, M. Hori, Non-thermal plasma-activated lactate solution kills U251SP glioblastoma cells in an innate reductive manner with altered metabolism, Arch. Biochem. Biophys. 688 (2020) 108414.
[32] K. Nakamura, N. Yoshikawa, M. Yoshihara, Y. Ikeda, A. Higashida, A. Niwa, T. Jindo, H. Tanaka, K. Ishikawa, M. Mizuno, S. Toyokuni, M. Hori, F. Kikkawa, H. Kajiyama, Adjusted multiple gases in the plasma flow induce differential antitumor potentials of plasma-activated solutions, Plasma Process. Polym. 17 (10) (2020).
[33] K. Nakamura, N. Yoshikawa, Y. Mizuno, M. Ito, H. Tanaka, M. Mizuno, S. Toyokuni, M. Hori, F. Kikkawa, H. Kajiyama, Preclinical verification of the efficacy and safety of aqueous plasma for ovarian cancer therapy, Cancers 13 (5) (2021) 1141.
[34] Z. Li, L. Jiang, S.H. Chew, T. Hirayama, Y. Sekido, S. Toyokuni, Carbonic anhydrase 9 confers resistance to ferroptosis/apoptosis in malignant mesothelioma under hypoxia, Redox Biol 26 (2019) 101297.
[35] H. Kojima, Y. Urano, K. Kikuchi, T. Higuchi, Y. Hirata, T. Nagano, Fluorescent indicators for imaging nitric oxide production, Angew Chem. Int. Ed. Engl. 38 (21) (1999) 3209–3212.
[36] H.R. McLennan, M. Degli Esposti, The contribution of mitochondrial respiratory complexes to the production of reactive oxygen species, J. Bioenerg. Biomembr. 32 (2) (2000) 153–162.
[37] G.P. Drummen, L.C. van Liebergen, J.A. Op den Kamp, J.A. Post, C11-BODIPY (581/591), an oxidation-sensitive fluorescent lipid peroxidation probe: (micro) spectroscopic characterization and validation of methodology, Free Radic. Biol. Med. 33 (4) (2002) 473–490.
[38] N. Kurake, H. Tanaka, K. Ishikawa, K. Takeda, H. Hashizume, K. Nakamura, H. Kajiyama, T. Kondo, F. Kikkawa, M. Mizuno, M. Hori, Effects of center dot OH and center dot NO radicals in the aqueous phase on H_2O_2 and NO_2^- generated in plasma-activated medium, J. Phys. D Appl. Phys. 50 (15) (2017) 155202.
[39] M. Lee, J.C. Choy, Positive feedback regulation of human inducible nitric-oxide synthase expression by Ras protein S-nitrosylation, J. Biol. Chem. 288 (22) (2013) 15677–15686.
[40] R. Radi, Oxygen radicals, nitric oxide, and peroxynitrite: redox pathways in molecular medicine, Proc. Natl. Acad. Sci. U. S. A. 115 (23) (2018) 5839–5848.
[41] M.I. Koukourakis, D. Kalamida, A. Giatromanolaki, C.E. Zois, E. Sivridis, S. Pouliliou, A. Mitrakas, K.C. Gatter, A.L. Harris, Autophagosome proteins LC3A, LC3B and LC3C have distinct subcellular distribution kinetics and expression in cancer cell lines, PloS One 10 (9) (2015), e0137675.
[42] X.T. Cheng, Y.X. Xie, B. Zhou, N. Huang, T. Farfel-Becker, Z.H. Sheng, Revisiting LAMP1 as a marker for degradative autophagy-lysosomal organelles in the nervous system, Autophagy 14 (8) (2018) 1472–1474.
[43] Y. Rabanal-Ruiz, E.G. Otten, V.I. Korolchuk, mTORC1 as the main gateway to autophagy, Essays Biochem. 61 (6) (2017) 565–584.
[44] G. Napolitano, A. Esposito, H. Choi, M. Matarese, V. Benedetti, C. Di Malta, J. Monfregola, D.L. Medina, J. Lippincott-Schwartz, A. Ballabio, mTOR-dependent phosphorylation controls TFEB nuclear export, Nat. Commun. 9 (2018) 3312.
[45] W.H. Zhang, X.Y. Li, S.J. Wang, Y.S. Chen, H.F. Liu, Regulation of TFEB activity and its potential as a therapeutic target against kidney diseases, Cell Death Dis. 6 (1) (2020) 32.
[46] Y. Ichimura, S. Waguri, Y. Sou, S. Kageyama, J. Hasegawa, R. Ishimura, T. Saito, Y. J. Yang, T. Kouno, T. Fukutomi, T. Hoshii, A. Hirao, K. Takagi, T. Mizushima, H. Motohashi, M.S. Lee, T. Yoshimori, K. Tanaka, M. Yamamoto, M. Komatsu, Phosphorylation of p62 activates the keap1-nrf2 pathway during selective autophagy, Mol. Cell. 51 (5) (2013) 618–631.
[47] A. Nasonova, H.C. Pham, D.J. Kim, K.S. Kim, NO and SO2 removal in non-thermal plasma reactor packed with glass beads-TiO2 thin film coated by PCVD process, Chem. Eng. J. 156 (3) (2010) 557–561.
[48] S. Toyokuni, F. Ito, K. Yamashita, Y. Okazaki, S. Akatsuka, Iron and thiol redox signaling in cancer: an exquisite balance to escape ferroptosis, Free Radic. Biol. Med. 108 (2017) 610–626.
[49] N.B. Janakiram, C.V. Rao, iNOS-selective inhibitors for cancer prevention: promise and progress, Future Med. Chem. 4 (17) (2012) 2193–2204.
[50] A.B. Levine, D. Punihaole, T.B. Levine, Characterization of the role of nitric oxide and its clinical applications, Cardiology 122 (1) (2012) 55–68.
[51] R. Chaleckis, I. Murakami, J. Takada, H. Kondoh, M. Yanagida, Individual variability in human blood metabolites identifies age-related differences, Proc. Natl. Acad. Sci. U. S. A. 113 (16) (2016) 4252–4259.
[52] B. Hinz, K. Brune, A. Pahl, Nitric oxide inhibits inducible nitric oxide synthase mRNA expression in RAW 264.7 macrophages, Biochem. Biophys. Res. Commun. 271 (2) (2000) 353–357.
[53] F. Vannini, K. Kashfi, N. Nath, The dual role of iNOS in cancer, Redox Biol 6 (2015) 334–343.
[54] B.K. Sinha, Nitric oxide: friend or foe in cancer chemotherapy and drug resistance: a perspective, J. Canc. Sci. Ther. 8 (2016) 244–251.
[55] T. Kallunki, O.D. Olsen, M. Jaattela, Cancer-associated lysosomal changes: friends or foes? Oncogene 32 (16) (2013) 1995–2004.
[56] R.A. Weber, F.S. Yen, S.P.V. Nicholson, H. Alwaseem, E.C. Bayraktar, M. Alam, R. C. Timson, K. La, M. Abu-Remaileh, H. Molina, K. Birsoy, Maintaining iron homeostasis is the key role of lysosomal acidity for cell proliferation, Mol. Cell. 77 (3) (2020) 645–655 e7.
[57] J.X. Bao, S. Jin, F. Zhang, Z.C. Wang, N. Li, P.L. Li, Activation of membrane NADPH oxidase associated with lysosome-targeted acid sphingomyelinase in coronary endothelial cells, Antioxidants Redox Signal. 12 (6) (2010) 703–712.
[58] T. Matsuzaki, A. Kano, T. Kamiya, H. Hara, T. Adachi, Enhanced ability of plasma-activated lactated Ringer's solution to induce A549 cell injury, Arch. Biochem. Biophys. 656 (2018) 19–30.
[59] B. Perillo, M. Di Donato, A. Pezone, E. Di Zazzo, P. Giovannelli, G. Galasso, G. Castoria, A. Migliaccio, ROS in cancer therapy: the bright side of the moon, Exp. Mol. Med. 52 (2) (2020) 192–203.
[60] T. Kimura, Y. Isaka, T. Yoshimori, Autophagy and kidney inflammation, Autophagy 13 (6) (2017) 997–1003.
[61] Y.F. Du, M.C. Wooten, M.W. Wooten, Oxidative damage to the promoter region of SQSTM1/p62 is common to neurodegenerative disease, Neurobiol. Dis. 35 (2) (2009) 302–310.
[62] W.Y. Wani, M. Boyer-Guittaut, M. Dodson, J. Chatham, V. Darley-Usmar, J. H. Zhang, Regulation of autophagy by protein post-translational modification, Lab. Invest. 95 (1) (2015) 14–25.
[63] Q. Qian, Z. Zhang, M. Li, K. Savage, D. Cheng, A.J. Rauckhorst, J.A. Ankrum, E. B. Taylor, W.X. Ding, Y. Xiao, H.J. Cao, L. Yang, Hepatic lysosomal iNOS activity impairs autophagy in obesity, Cell Mol Gastroenterol Hepatol 8 (1) (2019) 95–110.